Research paper

A detailed chemical kinetics model for the initial decomposition of gas-phase hydroxylamine

Yu-ichiro Izato*, Mitsuo Koshi**, and Atsumi Miyake*†

*Institute of advanced sciences, Yokohama National University
79-5 Tokiwadai, Hodogaya-ku, Yokohama 240-8501, JAPAN
Phone : +81-45-339-3993
†Corresponding author : miyake-atsumi-wp@ynu.ac.jp

**Graduate School of Environment and Information Sciences, Yokohama National University
79-7 Tokiwadai, Hodogaya-ku, Yokohama 240-8501, JAPAN

Received : July 27, 2016 Accepted : September 16, 2016

Abstract

Initial decomposition mechanisms of hydroxylamine in the gas phase were identified and investigated, and a detailed chemical kinetics model based on quantum chemical calculations was developed. The computational studies revealed the following reaction pathways : $2NH_2OH \rightarrow NH_3+HNO+H_2O$; $2NH_2OH \rightarrow t\text{-}N_2H_2+2H_2O$; and $NH_2OH+NH_3O \rightarrow NH_3+HNO+H_2O$. Optimized structures of reactants, products, and transition states were obtained at the ωB97XD/6-311++G(d,p) level of theory and the total electron energies of such structures were calculated at the CBS-QB3 level of theory. Detailed chemical reaction calculations revealed ignition of a thermal explosion after an induction period. The bimolecular reaction of NH_2OH occurs to yield HNO which attacks another NH_2OH to form N_2 and H_2O during the induction period. The series of reactions increases temperature and it promotes chain growth reactions, i.e., $NH_2OH+NH_2 \rightarrow NH_2O+NH_3$, and another chain initiation reaction, $HONO+M \rightarrow OH+NO+M$, activated radicals accumulate in the system. After sufficient radical accumulation, a thermal explosion is ignited and the temperature rises sharply to approximately 2400 °C.

Keywords : hydroxylamine, decomposition, runaway reaction, kinetic model, ***ab initio*** calculation

1. Introduction

Hydroxylamine (HA) is an oxygenated derivative of ammonia, represented by the chemical formula NH_2OH. It is an important reduction agent or antioxidant in the chemical and pharmaceutical industries[1)-5)]. In the semiconductor industry, HA solution is used in cleaning formulations to strip process residues from integrated circuit devices[6)]. In addition to these applications, HA is a primary material of hydroxylamine nitrate (HAN), a next generation rocket propellant oxidizer. HAN-based propellants are promising candidates as alternatives to toxic hydrazine-based propellants[7)].

Unfortunately, hydroxylamine is a potentially hazardous material[8)], and there have been two well-known major catastrophic explosions in the chemical industry involving HA : Pennsylvania, U.S. 1999 and Gunma, Japan 1999[9)]. For the safe use of HA including HAN-based propellants, it is important to understand the detailed reaction mechanisms of HA compositions and to develop an effective stabilizer for HA based on the knowledge of HA reactivity.

There have been many calorimetric studies and explosion hazard assessments for HA water solution[10)-20)], and some reasonable reaction mechanisms have been developed[21)-26)]. Hydroxylamine free base decomposes at high temperatures according to Equations. (1) and (2) in the ratios of 5/7 and 2/7, respectively[21),22)].

$$3NH_2OH \rightarrow N_2+NH_3+3H_2O \quad (1)$$
$$4NH_2OH \rightarrow N_2O+2NH_3+3H_2O \quad (2)$$

The initial step of hydroxylamine decomposition was proposed as the following[23)].

$$2NH_2OH \rightarrow NH_3+HNO+H_2O \quad (3)$$

Forming nitroxyl, HNO accelerates the HA decomposition and yields dinitrogen and dinitrogen oxide

as shown in the following equations[24].

$$NH_2OH + HNO \rightarrow N_2 + 2H_2O \quad (4)$$
$$2HNO \rightarrow N_2O + H_2O \quad (5)$$

These reactions are exothermic with heats of reaction of 451.6 kJ mol^{-1} and 366.9 kJ mol^{-1}, respectively[25], and cause runaway reactions through hazardous explosions. To prevent the hazardous runaway reaction of HA, the initial decomposition and accumulation of HNO must be inhibited based on knowledge of the reaction mechanisms. To the best of our knowledge, the detailed initial decomposition mechanisms, however, are still not completely clear. Wang et al.[26] reported that a transition state could not be located for reaction (3), which implied that this reaction may not be an elementary reaction. Wang et al.[26),27] advocated that NH_3O, an isomer of HA, plays an important role in the initial decomposition, and the reaction $NH_3O + H_2O \rightarrow NH_3 + H_2O_2$ is a feasible reaction in the initial decomposition pathway. They also calculated the dissociation enthalpy of NH_3O ($NH_3O \rightarrow NH_3 + {}^3O$) to be 35 kcal mol^{-1} at the G2 level of theory[27]. The dissociation reaction, however, is a spin-forbidden reaction and does not proceed directly.

In this study, to gain a better understanding of HA reactivity, initial decomposition pathways of HA in the gas phase were investigated on the basis of *ab initio* calculations. This approach is helpful with regard to determining the reactions that should be excluded from the mechanism based on thermodynamic arguments. There have been previous studies that have taken an *ab initio* approach to studying the reactions of HA[21),25)–27]. These, however, have not identified or developed mechanisms of HA bimolecular reactions. After studies based on *ab initio* computations, we modeled the kinetics of HA initial decomposition, and investigated the reaction process using detailed chemical reaction calculations.

2. Computational

The geometries of the reactants, products, and transition states were optimized at the ωB97XD/6-311++G(d,p) level[28] of theory using the Gaussian 09 program package[29]. Gordon et al. developed the ωB97XD method, which includes empirical dispersion forces and is believed to be reliable when applied to systems with weak van der Waals forces[28]. Their group also reported that the ωB97XD method yields satisfactory accuracy for kinetics and non-covalent interactions[28].

During computations, transition states (TSs) were extensively searched for and, if found, an intrinsic reaction coordinate (IRC) calculation was conducted in order to assign reactants and products to the TS.

The energies of corresponding molecules were evaluated at the CBS-QB3[30] level of theory, since this is a reasonable time-expense complete basis method. In this study, geometries and frequencies were calculated at the ωB97XD/6-311++G(d,p) level, the optimized geometries were fixed with no changes allowed and the energies were calculated using the CBS-QB3 method. CBS-QB3 is understood to represent cost-effective strategies for obtaining chemically accurate thermochemical calculations.

Transition state theory calculations were also performed to obtain the rate coefficient by using the Gaussian postprocessor (GPOP) program suite[31] developed by Miyoshi[32)–34]. GPOP is a collection of tools for the estimation of thermodynamics and rate coefficients for gas-phase reactions.

We obtained thermodynamic data for some chemical species that are not listed in existing databases[35),36] based on the G4 level of theory[37]. The structures and energies were elaborated to obtain thermodynamic data using the GPOP program suite[31].

3. Results and discussion

3.1 Molecular structures and thermodynamic data

Figure 1 illustrates important chemical species in HA decomposition mechanism. Table 1 lists data collection of thermodynamic data for NH_3O, NH_2NH_2O, and $NH_2(O)OH$. To conduct detailed chemical reaction simulation, these data is essential. There, however, are no data such species in published data base[35),36].

3.2 Decomposition mechanisms of HA

Bimolecular reactions of HA in the gas phase were identified and investigated.

$$NH_2OH + NH_2OH \rightarrow NH_3 + HNO + H_2O \quad (6)$$
$$NH_2OH + NH_2OH \rightarrow 2H_2O + t\text{-}N_2H_2 \quad (7)$$

Figure 2 shows potential energy profiles including the optimized structures of transition states for the initial

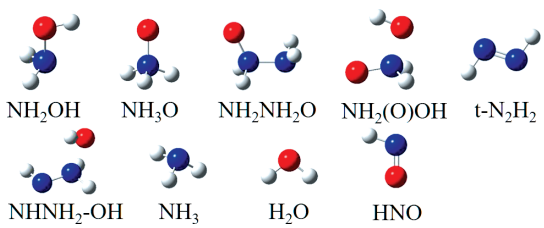

Figure 1 Chemical structures of reactants, products and intermediates in HA decomposition as optimized at the ωB97XD/6-311++G(d,p) level of theory.

Table 1 Thermodynamic data of chemical species in HA decomposition mechanism. Quantum chemistry calculation results at the G4 level of theory were elaborated to obtain thermodynamic data. unit system : H_{298} [kJ mol^{-1}] S_{298} [J K^{-1} mol^{-1}] C_P [J K^{-1} mol^{-1}]

Species	H298	S298	$Cp_{,298}$	$Cp_{,300}$	$Cp_{,400}$	$Cp_{,500}$	$Cp_{,600}$	$Cp_{,800}$	$Cp_{,1000}$	$Cp_{,1500}$
NH3O	10.13	235.96	37.27	37.36	43.33	49.95	56.27	67.09	75.55	89.04
NH2NH2O	12.15	265.28	54.05	54.25	65.52	76.30	85.78	100.97	112.42	130.73
NH2(O)OH	12.67	269.01	54.22	54.38	63.11	71.43	78.69	90.14	98.66	112.29

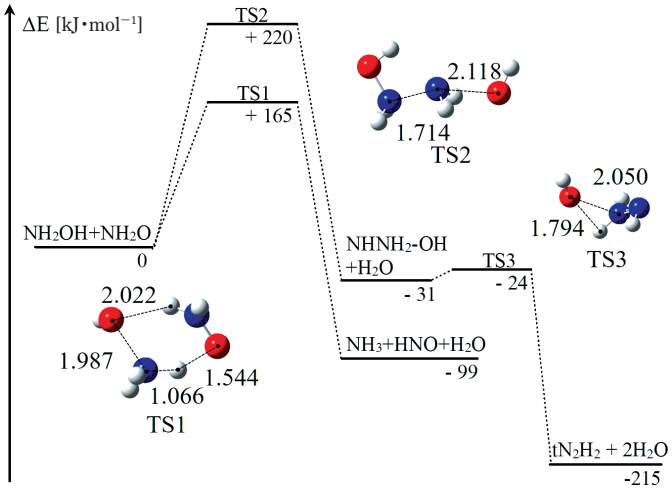

Figure 2 Potential energy profiles for the bimolecular reaction $NH_2OH + NH_2OH \rightarrow NH_2O\text{-}OH + NH_3$. The energy profiles were calculated at the CBS-QB3//ω B97XD/6-311++G(d,p) level of theory.

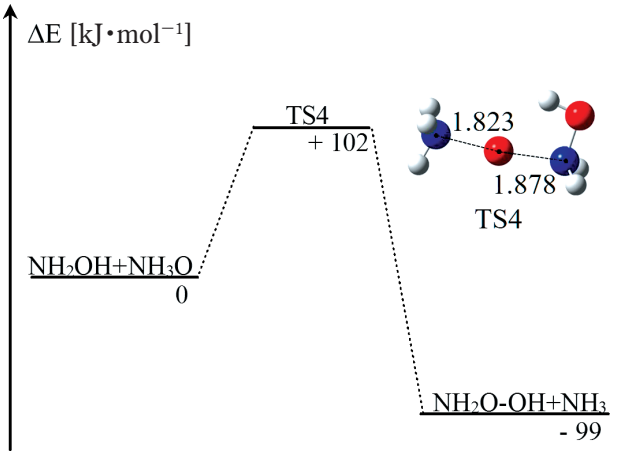

Figure 3 Potential energy profiles for the bimolecular reaction $NH_2OH + NH_3O \rightarrow NH_2(O)OH + NH_3$. The energy profiles were calculated at the CBS-QB3//ω B97XD/6-311++G(d,p) level of theory.

bimolecular reactions of HA. In the mechanism via TS1, cleavage of the N-O bond in one HA triggers decomposition and the NH_2 dissociated from the HA abstracts H from -OH in the other HA, temporarily producing NH_3 and NH_2O. Subsequently, the other dissociated OH abstracts H from NH_2O, producing HNO and H_2O. The energy barrier height is calculated as 165 kJ mol^{-1} at the CBS-QB3//ωB97XD/6-311++G(d,p) level of theory. Wang et al.[26] reported transition states could not be located for the reaction (6), which implied that this reaction may not be an elementary one. This study, however, revealed and identified one such transition state.

In the mechanism via TS2, decomposition also starts from cleavage of the N-O bond of one HA. The NH_2 dissociated from the HA binds NH_2- in the other HA to produce OH and NH_2NH_2OH temporarily. The dissociated OH abstracts hydrogen from NH_2- in the NH_2NH_2OH to produce an intermediate complex of H_2O and $NHNH_2$-OH. The energy barrier height is calculated as 220 kJ mol^{-1} at the CBS-QB3//ωB97XD/6-311++G(d,p) level of theory. Subsequently, $NHNH_2$-OH decomposes to *trans*-diazene, t-N_2H_2, through hydrogen transfer from $NHNH_2$- to -OH. The energy barrier height of 7 kJ mol^{-1} is considered to be negligible compared with the former step.

Wang et al.[26),27)] advocated that NH_3O, an isomer of HA, played an important role in the initial decomposition. In this study, reactions relating to NH_3O as shown in the following were identified and investigated.

$$NH_2OH+NH_3O \rightarrow NH_2(O)OH+NH_3 \quad (8)$$

Figure 3 shows potential energy profiles including optimized structures of transition states for this reaction. The reaction starts from cleavage of the N-O bond of NH_3O and the O binds NH_2- in the other HA to yield NH_3 and $NH_2(O)OH$. $NH_2(O)OH$ decomposes to yield HNO and H_2O, as will be discussed later. The complete reaction is represented by $NH_2OH+NH_3O \rightarrow HNO+NH_3+H_2O$. The energy barrier height is calculated to be 102 kJ mol^{-1} at the CBS-QB3//ωB97XD/6-311++G(d,p) level of theory. Due to the lower energy barrier compared with bimolecular reactions of HA, this mechanism is a preferable candidate for the decomposition of HA in the presence of NH_3O.

In this study, we also identified and investigated a trimolecular reaction involving a third NH_2OH, as shown below.

$$NH_2OH+NH_2OH+NH_2OH \rightarrow NH_2NH_2O+NH_3O+H_2O \quad (12)$$

The schematic potential energy surface of these reactions is shown in Figure 4. This trimolecular mechanism has a lower energy barrier of 123 kJ mol^{-1} compared to the bimolecular reactions of 165 and 220 kJ mol^{-1}. In this mechanism, the third HA plays a hydrogen transfer carrier role. After initial cleavage of the N-O bond of one HA, $NH_2OH \rightarrow NH_2$+OH, the hydrogen transfers from -OH in the third HA to the dissociated OH to form H_2O and NH_2O, and then the other dissociated NH_2 binds the second HA to form NH_2NH_2OH. NH_2O originating from the third HA subsequently abstracts hydrogen from -OH in NH_2NH_2OH to yield NH_3O and NH_2NH_2O, as shown in TS5 in Figure 4. Finally, NH_2NH_2O, H_2O, and NH_3O are produced. HA has a self-catalytic mechanism, because NH_3O can isomerize and reproduce NH_2OH exothermically. This isomerization mechanism is well investigated on the basis of *ab initio* calculations in References.[26),27),38),39)].

It was found that water molecules assist the decomposition of HA, as shown in the following.

$$NH_2OH+NH_2OH+H_2O \rightarrow NH_2NH_2O+2H_2O \quad (10)$$

In the present study, we identified and investigated ring transition states, and the schematic potential energy surface of these reactions is shown in Figure 5. After initial cleavage of the N-O bond of HA, the H_2O molecule acts as a carrier for hydrogen transfer from OH in NH_2NH_2-OH to dissociate OH, as shown in TS6 in Figure 5. Reactions in which water molecules serve as hydrogen transfer agents are common. Transition states proposed in the absence of explicit solvent molecules typically involve highly strained rings, since these are necessary to transfer the hydrogen from one position in the molecule to another. The result is

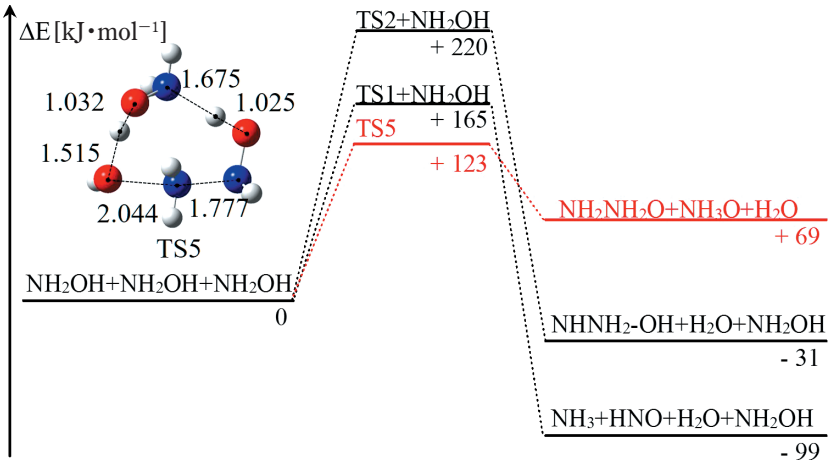

Figure 4 Potential energy profiles for trimolecular reaction of HA. The energy profiles were calculated at the CBS-QB3//ωB97XD/6-311++G(d,p) level of theory.

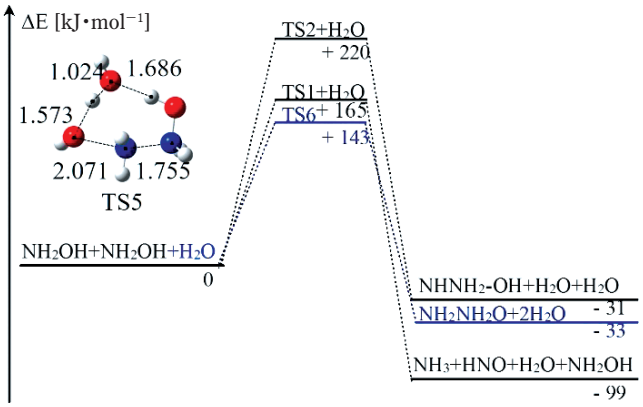

Figure 5 Potential energy profiles for water-catalyzed reaction of HA. The energy profiles were calculated at the CBS-QB3//ωB97XD/6-311++G(d,p) level of theory.

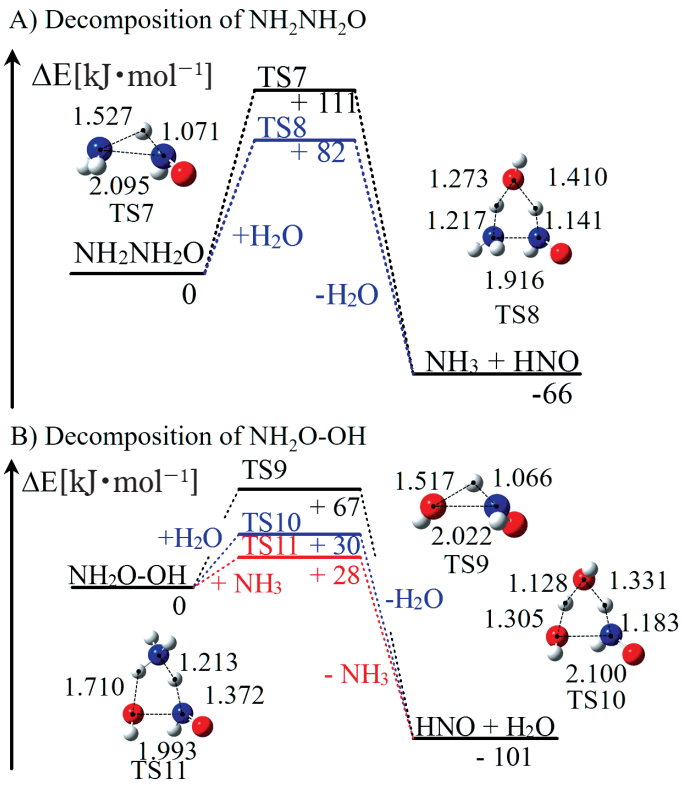

Figure 6 Potential energy profiles for decomposition of intermediates NH_2NH_2O A) and $NH_2(O)OH$ B). The energy profiles were calculated at the CBS-QB3//ωB97XD/6-311++G(d,p) level of theory.

usually a high energetic barrier to the reaction. The inclusion of solvent molecules allows the ring structure to be larger and less strained, reducing the transition state energy compared to a small, cyclic transition state structure. Here, one or more water molecules simultaneously accept a hydrogen atom at a lone pair site and give up one of the original hydrogen atoms to another molecule.

NH_2NH_2O and $NH_2(O)OH$ are intermediates in the initial HA decomposition discussed above. We identified and investigated the decomposition of these intermediates, as shown below.

$$NH_2NH_2O \rightarrow NH_3+HNO \quad (14)$$
$$NH_2(O)OH \rightarrow H_2O+HNO \quad (15)$$

The schematic potential energy surface of these reactions and optimized structures of transition states, reactants, and products are shown in Figure 6. Here, water molecules also assist in the intramolecular hydrogen transfer of NH_2NH_2O and $NH_2(O)OH$ in a manner that makes a ring structure and transfers a hydrogen, as in TS 9 and TS11. Although the unimolecular decompositions have a relatively high energy barrier of 111 kJ mol^{-1} (NH_2NH_2O) and 67 kJ mol^{-1} ($NH_2(O)OH$), water-catalysis effects decreased these to 82 kJ mol^{-1} (NH_2NH_2O) and 30 kJ mol^{-1} ($NH_2(O)OH$), respectively. NH_3 also has a catalytic role in the decomposition of $NH_2(O)OH$ and it decreases the energy barrier height to 28 kJ mol^{-1}.

3.3 Kinetic models of initial decomposition of hydroxylamine

We modeled the kinetics of the HA initial decomposition discussed above on the basis of transition state theory, and listed them in Table 2. We constructed the YNU01 model in this study. A chemical kinetics mechanism for HA decomposition has been developed by modifying the UT06 mechanism originally proposed by Daimon et al.[40]. This mechanism consists of 33 species and 239 reactions. Most of the elementary reactions for N-H species and their rate

Table 2 Kinetics models for HA initial decomposition reactions.

No.	Reaction	Energy change[a] ΔE_0		Rate coefficient[b] $k(T) = AT^n \exp\left(-\frac{E_a}{RT}\right)$		
		TS	Product	A [1]	n	ΔE_a/R
1	$NH_2OH+NH_2OH \rightleftharpoons HNO+NH_3+H_2O$	165.2	−99.4	4.08×10^{-1}	3.71	19165
2	$NH_2OH+NH_2OH \rightleftharpoons t\text{-}N_2H_2+2H_2O$	220.4	−200.2	5.21×10^{-1}	3.52	25551
3	$NH_2OH+NH_2OH+H_2O \rightleftharpoons NH_2NH_2O+2H_2O$	143.2	−33.1	3.48×10^{-12}	5.99	14902
4	$NH_2OH+NH_2OH+NH_2OH \rightleftharpoons NH_2NH_2O+NH_3O+H_2O$	122.7	69.0	2.76×10^{-13}	6.01	12607
5	$NH_2OH+NH_3O \rightleftharpoons NH_3+NH_2(O)OH$	101.9	−99.8	1.52×10^{1}	3.53	11619
6	$NH_2NH_2O \rightleftharpoons HNO+NH_3$	111.3	−66.3	4.02×10^{9}	1.45	12922
7	$NH_2NH_2O+H_2O \rightleftharpoons HNO+NH_3$	81.5	−66.3	2.70×10^{-4}	4.52	7234
8	$NH_2(O)OH \rightleftharpoons HNO+H_2O$	67.4	−101.6	6.25×10^{10}	0.94	7897
9	$NH_2(O)OH+H_2O \rightleftharpoons HNO+2H_2O$	30.2	−101.6	3.03×10^{-3}	4.15	1386
10	$NH_2(O)OH+NH_3 \rightleftharpoons HNO+H_2O+NH_3$	29.0	−101.6	2.66×10^{-1}	3.72	2134
11	$NH_2OH \rightleftharpoons NH_3O$	205.7	102.0	1.99×10^{5}	2.24	22139

[a] unit system is kJ mol^{-1} [b] Unimolecular rate coefficients in s^{-1} ; bimolecular rate coefficients in $cm^3\ mol^{-1}\ s^{-1}$; trimolecular rate coefficients in $cm^6\ mol^{-2}\ s^{-1}$.

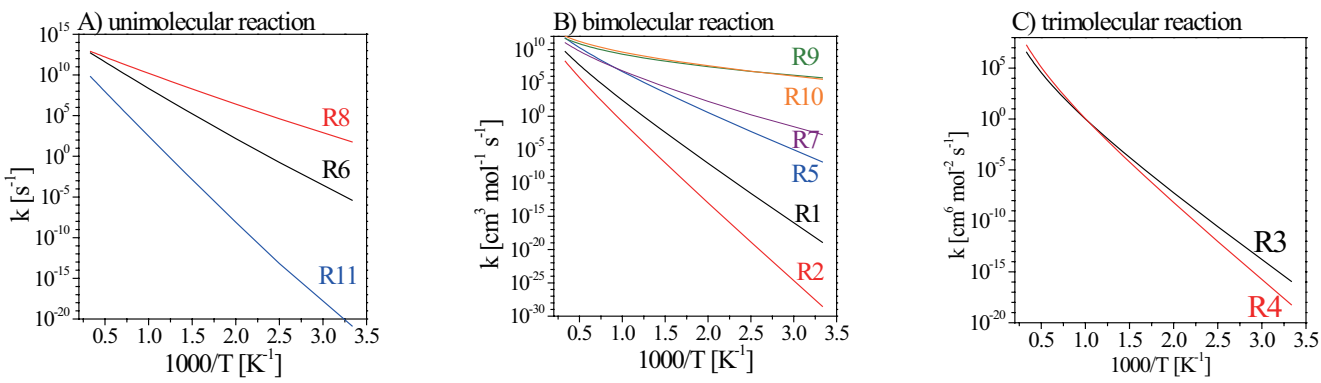

Figure 7 Rate coefficients for the HA decomposition reactions listed in Table 2. A) shows rate coefficients for the unimolecular reaction, B) shows rate coefficients for the bimolecular reaction, C) shows rate coefficients for the trimolecular reaction.

coefficients in the mechanism are taken from Dean and Bozzelli[41]. The reaction $NH_2+OH \rightleftharpoons NH_2OH$ is taken from the NIST kinetics database[42]. The subset of hydrogen combustion is replaced by a recent mechanism[43], which is appropriate for high-pressure conditions. Figure 7 depicts the temperature dependence of the respective rate coefficients listed in Table 2.

3.4 Detailed chemical reaction simulation

To gain a better understanding of the ignition process of HA decomposition, the YNU01 mechanism revealed an ignition delay time of a NH_2OH/H_2O=9/1 gas mixture at P=1 atm under adiabatic combustion (constant enthalpy and pressure). We used the CHEMKIN-PRO program suite[44] for the calculation. There are some differences between practical HA decomposition conditions and the calculation condition presented in this paper. HA is usually handled as an aqueous solution[8]. HA crystals and solutions are known to explosively decompose at concentrations of higher than 80 wt.%[16]. Practical HA decomposition occurs in the condensed phase, but this calculation can only be used to analyze a gas-phase reaction. It must be noted that this difference may have a significant influence on the analysis. However, we believe that the calculation results for the gas-phase reaction can provide some insight into the HA ignition process.

An example of temperature and species time profiles at an initial temperature of T=600 °C is shown in Figure 8. An abrupt rise in temperature at approximately 65 s in Figure 8 clearly indicates the ignition. It is noted that the temperature gradually increases during the induction period. Temporal profiles of major species and radicals are also depicted in Figure 8. In the induction period, the concentration of HNO, NH_3 and increases at first, and then N_2, NO, N_2O, HONO and NO_2 are produced. Production of NH_3 and HNO is the result of reactions 1 in Table 2.

We illustrate the decomposition pathways as follows. The bimolecular reaction of NH_2OH occurs during the

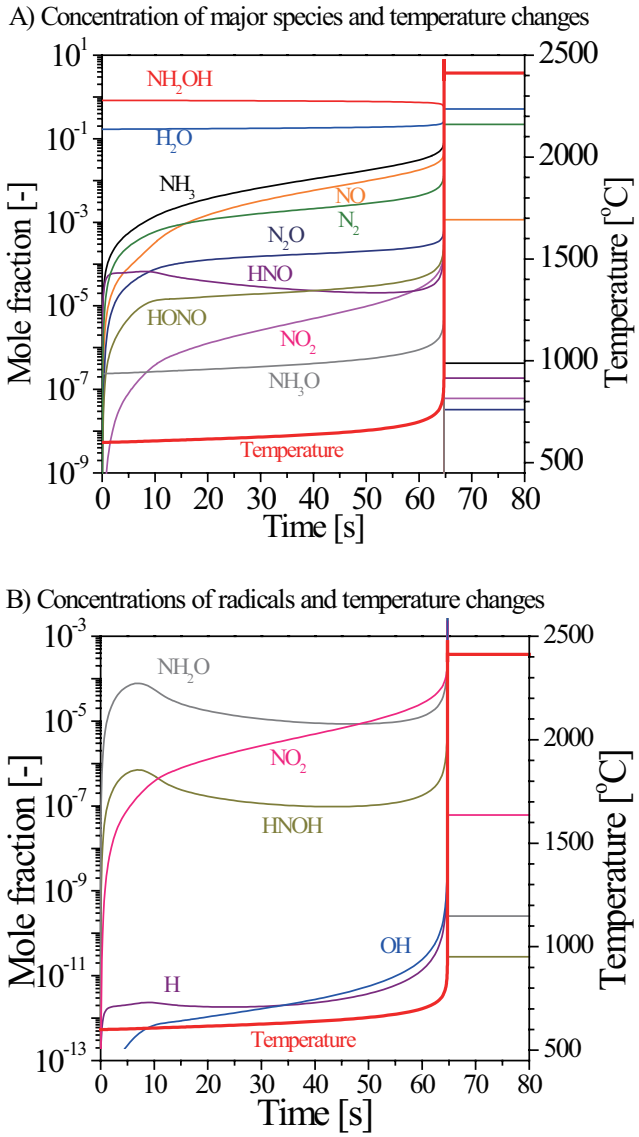

Figure 8 Temperature and species time histories of NH_2OH/H_2O = 9/1 mixture at $P_0 = 1$ atm and $T_0 = 600$ °C under the adiabatic and constant pressure condition. The upper graph A) shows concentration of major species and temperature changes and the lower graph B) shows concentration of radicals and temperature changes.

induction period. Figure 9 shows the absolute rate of NH_2OH production at time of 30 s calculated by reaction path analysis in the CHEMKIN-PRO program suite[43]. NH_2OH mainly decompose to HNO, NH_3 and, H_2O in the bimolecular reaction. The HNO react with NH_2OH to yield N_2 and H_2O as in the equation $NH_2OH+HNO \rightarrow N_2+2H_2O$, which then increase the temperature. HNO also decomposes to N_2O and H_2O in the reaction $HNO+HNO \rightarrow N_2O+H_2O$ with exothermic heat. As a result of increasing in temperature, through subsequent chain growth reactions, i.e., $NH_2OH+OH \rightarrow H_2O+NH_2O$; $NH_2OH+OH \rightarrow H_2O+NHOH$; $NH_2OH+NH_2 \rightarrow NH_2O+NH_3$: and $NH_2OH+NH_2 \rightarrow NHOH+NH_3$ and other chain initiation reactions, $HONO+M \rightarrow OH+NO+M$ and $HNO+M \rightarrow H+NO+M$, activated radicals gradually accumulate in the system as shown in Figure 8. After sufficient radical accumulation, a thermal explosion is ignited and the temperature rises to approximately 2400 °C. From results of reaction path

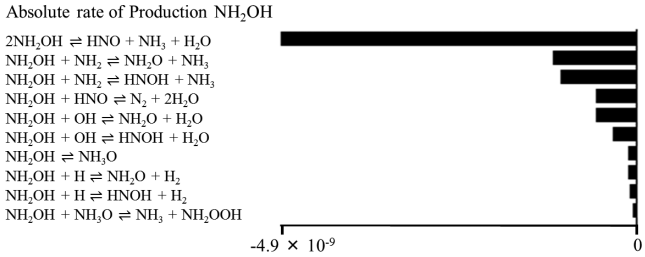

Figure 9 Absolute rate of NH_2OH production at time = 30 s and T_{30} = 627 °C, calculated on the basis of the YNU 01 model by CHEMKIN-PRO.

analysis, NH_3O which is the isomer of NH_2OH did not play important role in decomposition of NH_2OH in gas phase.

4. Conclusions

The initial decomposition pathway of HA in the gas phase was investigated on the basis of *ab initio* calculations. The calculations were performed at the ωB97XD/6-311++G(d,p) and CBS-QB3//ωB97XD/6-311++G(d,p) level of theories. Mechanisms for the bimolecular reactions $2NH_2OH \rightarrow NH_3+HNO+H_2O$, $2NH_2OH \rightarrow t\text{-}N_2H_2+H_2O$, and $NH_2OH+NH_3O \rightarrow NH_3+HNO+H_2O$ were also developed. Maximum energy barrier heights for each reaction were calculated as 165 kJ mol^{-1}, 220 kJ mol^{-1}, and 102 kJ mol^{-1}, respectively. The presence of water and a third HA assisted the decomposition, $2NH_2OH \rightarrow NH_3+HNO+H_2O$, and decreased energy barrier heights, which were calculated as 103 kJ mol^{-1} (third HA-catalyzed) and 127 kJ mol^{-1} (water-catalyzed), respectively. We modeled these reactions of kinetics and developed the YNU01 model. Detailed chemical reaction simulations revealed that the thermal explosion occurs after an induction period. The bimolecular reaction, $NH_2OH+NH_2OH \rightarrow HNO+NH_3+H_2O$, starts the decomposition reaction, and then the HNO attacks NH_2OH to yield N_2 and H_2O with exothermic heat during the induction period. The HNO also exothermically decompose to N_2O and H_2O and the temperature increases gradually. As a result of increasing in temperature, through subsequent chain growth reactions, i.e., $NH_2OH+NH_2 \rightarrow NH_2O+NH_3$, and another chain initiation reaction, $HONO+M \rightarrow OH+NO+M$, activated radicals gradually accumulate in the system. After sufficient radical accumulation, a thermal explosion is ignited and the temperature rises sharply.

Acknowledgement

This research was supported by the Foundation for the Promotion of Industrial Explosives Technology 2015.

5. References

1) R. Mokaya and M. Poliakoff, NATURE, 437, 1243−1244 (2005).
2) G. Bellussi and C. Perego, CATTECH, 4, 4−16 (2000).
3) J. J. Sahbari and J. W. Russell, US patent, 148, 305−309 (2001).
4) F. Zhao, K. You K, C. Peng, S. Tan, R. Li, P. Liu, J. Wu, and H. Luo, Chem. Eng. Journal, 272, 102−107 (2015).
5) S. Hallam and P. Wilkinson, IcheE Symposia Series, 148, 305−309 (2001).

6) K. A. Reinhardt and R. F. Reidy, "Handbook for Cleaning for Semiconductor Manufacturing: Fundamentals and Applications", Wiley, 344–347 (2010).
7) T. Katsumi, T. Inoue, J. Nakatsuka, K. Hasegawa, K. Kobayashi, S. Sawai, and K. Hori, Combust, Explos, Shock Waves, 48, 536–543 (2012).
8) L. A. Long, Process Safety Process, 23, 114–120 (2004).
9) P. G. Urben ed., "6 ed. Bretherick's Handbook of Reactive Chemical Hazards" vol. 1, 1662–1664, Butterworth-Heinemann Ltd (1995).
10) C. Wei, W. J. Rogers, and M. S. Mannan, J. Hazz. Mater., 130, 163–168 (2006).
11) C. Wei, W. J. Rogers, and M. S. Mannan, Thermochimica Acta, 421, 1–9 (2004).
12) T. Adamopoulou, M. I. Papadaki, M. Kounalakis, V. Vazquez -Carreto, A. Pineda-Solano, Q. Wang, and M. S. Mannan, J. Hazzard. Mater., 254–255, 382–389 (2013).
13) L. Liu, M. Papadaki, E. Pontiki, P. Stathi, W. J. Rogers, and M. S. Mannan, J. Hazzard. Mater., 165, 382–389 (2009).
14) M. Papadaki, E. Pontiki, L. Liu, W. J. Rogers, and M. S. Mannan, J.Chem. Eng. Data, 54, 2616–2621 (2009).
15) T. Adamopoulou, M. I. Papadaki, M. Kounalakis, V. Carreto, A. Pienda, and M. S. Mannan, J.Loss Prev. Process Ind., 25, 803–808 (2012).
16) Y. Iwata and H. Koseki, Process Saf. Prog., 21, 136–141 (2002).
17) Y. Iwata, H. Koseki, and F. Hosoya, J.Loss Prev. Process Ind., 216, 41–53 (2003).
18) M. Kumasaki, J. Hazzard. Mater., 115, 57–62 (2004).
19) M. Kumasaki, Y. Fujimoto, and T. Ando, J. Loss Prev. Process Ind., 16, 507–512 (2003).
20) K. A. Hofmann and F. Kroll, Berichte, 57B, 937–944 (1924) (in German).
21) G. E. Alluisetti, A. E. Almaraz, V. T. Amorebieta, F. Doctorovich, and J. A. Olabe, J. Am. Chem. Soc. 2004, 126, 13432–13442
22) V. R. Nast and I. Z. Föppl, Anorg. Allg. Chem., 263, 310–315 (1950).
23) F. T. Bonner, L. S. Dzelzkalns, and J. A. Bonucci, Inorg. Chem., 17, 2487–2494 (1978).
24) C. Wei, S. R. Saraf, W. J. Rogers, and M. S. Mannan, Thermochimica Acta, 421, 1–9 (2004).
25) J. M. Bremner, A. M. Blackmer, and S. A. Waring, Soil Biol. Biochem, 12, 263–269 (1980).
26) Q. Wang, C. Wei, L. M. Pe'rez, W. J. Rogers, M. B. Hall, and M. S. Mannan, J. Phys. Chem. A, 114, 9262–9269 (2010).
27) Q. Wang and M. S. Mannan, J. Chem. Eng. Data, 55, 5128–5132 (2010).
28) J. D. Chai and M. Head–Gordon, Phys. Chem. Chem. Phys. 10, 6615–6620 (2008)
29) M. J. Frisch, G. W. Trucks, H. B. Schlegel, G. E. Scuseria, M. A. Robb, J. R. Cheeseman, G. Scalmani, V. Barone, B. Mennucci, G. A. Petersson, H. Nakatsuji, M. Caricato, X. Li, H. P. Hratchian, A. F. Izmaylov, J. Bloino, G. Zheng, J. L. Sonnenberg, M. Hada, M. Ehara, K. Toyota, R. Fukuda, J. Hasegawa, M. Ishida, T. Nakajima, Y. Honda, O. Kitao, H. Nakai, T. Vreven, J. A. Montgomery, J. E. Peralta, F. Ogliaro, M. Bearpark, J. J. Heyd, E. Brothers, K. N. Kudin, V. N. Staroverov, T. Keith, R. Kobayashi, J. Normand, K. Raghavachari, A. Rendell, J. C. Burant, S. S. Iyengar, J. Tomasi, M. Cossi, N. Rega, J. M. Millam, M. Klene, J. E. Knox, J. B. Cross, V. Bakken, C. Adamo, J. Jaramillo, R. Gomperts, R. E. Stratmann, O. Yazyev, A. J. Austin, R. Cammi, C. Pomelli, J. W. Ochterski, R. L. Martin, K. Morokuma, V. G. Zakrzewski, G. A. Voth, P. Salvador, J. J. Dannenberg, S. Dapprich, A. D. Daniels, O. Farkas, J. B. Foresman, J. V. Ortiz, J. Cioslowski, and D. J. Fox, Gaussian 09, Revision D.01, Gaussian, Inc., Wallingford CT (2010).
30) J. A. Montgomery, M. J. Frisch, J. W. Ochterski, and G. A. Petersson, J. Chem. Phys., 110, 2822–2827 (1999).
31) A. Miyoshi, GPOP software, rev. 2013.07.15 m5, available from the author. See http://www.frad.t.u-tokyo.ac.jp/~miyoshi/gpop/.
32) A. Miyoshi, International Journal of Chemical Kinetics, 42, 273–288 (2010).
33) A. Miyoshi, J. Phys. Chem. A, 115, 3301–3325 (2011).
34) A. Miyoshi, International Journal of Chemical Kinetics, 44, 59–74 (2012).
35) R. J. Kee, F. M. Rupley, and J. A. Miller, "The Chemkin Thermodynamic Data Base", Sandia National Laboratories Report SAND87–8215B (1990).
36) A. Burcat and B. Ruscic, "Third Millennium Ideal Gas and Condensed Phase Thermochemical Database for Combustion with Updates from Active Thermochemical Tables", ANL–05/20, TAE960 (2005).
37) L. A. Curtiss, P. C. Redfern, and K. Raghavachari, J. Chem. Phys. 126, 084108 (2007).
38) G. F. de Lima, J. R. Piego Jr, and H. A. Duarte, Chem. Phys. Lett., 518, 61–64 (2011).
39) M. I. Fernádez, M. Canle, M. V. García, and J. A. Santaballa, Chem. Phys. Lett., 490, 159–164 (2010).
40) Y. Daimon, H. Terashima, and M. Koshi, J. Propul. Power, 30, 707–716 (2014).
41) A. M. Dean, J. W. Bozzelli, and W. C. Gardiner Jr edited, " Gas-Phase Combustion Chemistry", 125–316, Springer-Verlag, New York (2000).
42) NIST Chemical Kinetics Database, Standard Reference Database 17, Version 7.0 (Web Version), Release 1.6.8 Data Version 2015.12 (accessed : 28-July- 2016) (online).
43) K. Shimizu, A. Hibi, M. Koshi, Y. Morii, and N. Tsuboi, J. Propul. Power, 27, 383–395 (2011).
44) CHEMKIN-Pro Input Manual PRO-INP-15092-UG-1, Reaction Design, San Diego, CA, (2011).